

Electronic structure of two-dimensional hexagonal diselenides: charge density waves and pseudogap behavior

¹E.Z. Kuchinskii, ¹I.A. Nekrasov, ^{1,2}M.V. Sadovskii

¹*Institute for Electrophysics, Russian Academy of Sciences, Ural Branch,
Amundsen str. 106, Ekaterinburg, 620016, Russia*

²*Institute for Metal Physics, Russian Academy of Sciences, Ural Branch,
S. Kovalevskaya str. 18, Ekaterinburg, 620219, Russia*

Abstract

We present theoretical study of electronic structure (spectral functions and Fermi surfaces) for incommensurate pseudogap and charge density wave (CDW) and commensurate CDW phases of quasi two dimensional diselenides 2H-TaSe₂ and 2H-NbSe₂. Incommensurate pseudogap regime is described within the scenario based on short-range order CDW fluctuations, considered within the static Gaussian random field model. In contrast e.g. to high-T_c cuprates layered dichalcogenides have several different CDW scattering vectors and electronic spectrum with two bands at the Fermi level. To this end we present theoretical background for the description of multiple scattering processes within multiple bands electronic spectrum. Thus obtained theoretical spectral functions and Fermi surfaces are compared with recent ARPES experimental data, demonstrating rather good qualitative agreement.

PACS numbers: 71.10.Hf, 71.30.+h, 71.45.Lr

INTRODUCTION

Quasi-two-dimensional dichalcogenides TX_2 ($\text{T}=\text{Nb},\text{Ta},\text{Mo},\text{Hf}$; $\text{X}=\text{S},\text{Se}$) and their different polymorphic modifications long time ago attracted the attention of scientific community [1]. This was connected with: (i) early suggestions to look for high- T_c superconductivity in layered compounds; (ii) the discovery of phase transitions with formation of charge density waves (CDW) [1]. In particular, in 2H-TaSe₂ (2H means – hexagonal structure with two Ta layers in the unitcell) the second order transition into incommensurate CDW phase is observed at temperature =122.3K. At 90K there is another transition to commensurate CDW phase [1, 2]. In 2H-NbSe₂ transition to incommensurate CDW phase happens at much lower temperature of 33.5K [2] and no commensurate CDW phase is observed.

Above the temperature of incommensurate CDW transition in these systems there might be the range of temperatures where short-range order CDW fluctuations with finite, but pretty large, correlation length ξ may exist due to low-dimensional nature of these systems (and in analogy with antiferromagnetic fluctuations in cuprates). This indeed is experimentally observed in angular resolved X-ray photoemission (ARPES) experiments [3–5].

In this paper we present band structure calculation results for 2H-TaSe₂ and 2H-NbSe₂ with analysis of possible topologies of the Fermi surfaces upon doping, showing possibility of formation of “bone”- like Fermi sheets. Further we describe the details of theoretical description of multiband electronic multiple scattering on CDW in a multiple band systems, as applied to pseudogap, incommensurate and commensurate CDW phases for both 2H-TaSe₂ and 2H-NbSe₂. As an outcome, we obtain spectral functions and Fermi surface maps, which are compared with a number of recent ARPES results [3, 4].

BAND STRUCTURE

The 2H-TX₂ layered compounds have hexagonal crystal structure with the space group of symmetry $P6_3/mmc$ with lattice parameters for Ta system $a=3.436 \text{ \AA}$ and $c=12.7 \text{ \AA}$. Corresponding Wyckoff positions are for Ta 2b (0,0,0.25) and Se 4f ($\frac{1}{3},\frac{2}{3},0.118$) [2]. Formal electronic configuration of Ta is d^1 . To calculate electronic structure of the compound the linearized muffin-tin orbitals method (LMTO) [6] with default settings was employed. Obtained band structure and Fermi surfaces are in good agreement with similar LDA cal-

culations by other authors [7]. We do not present any LDA results on 2H-NbSe₂ since its crystal structure [2] and corresponding band structure are very close to those of 2H-TaSe₂.

In accord with the previous works [7] in our LDA calculations the Fermi level in 2H-TaSe₂ is crossed by two Ta-5d bands with $3z^2 - r^2$ symmetry (see Fig. 1a), which are well separated from other bands.

Fermi surface (FS) of 2H-TaSe₂ has three (in some works two [7]) hole-like cylinders near the Γ -point and two hole cylinders around K-point. Our results are presented in Fig. 1b. Here we observe three hole-like cylinders around the Γ -point.

During the recent years several ARPES studies detected the experimental FS of 2H-TaSe₂. In particular, in Ref. [8] the electronic structure of the valence band was studied in 1T-TaS₂ and 2H-TaSe₂. For 2H-TaSe₂ it was shown that along Γ -K direction there are four crossings with the FS. Similar picture is also seen in LDA results (Fig. 1a,b). In later ARPES works [3, 4, 9] it was observed that FS of 2H-TaSe₂ has more complex topology. Namely, along Γ -K direction there appear the “bone”-like FS sheets. Within the LDA picture one can obtain such “bones” by the shift of the Fermi level down by about 0.1 eV (Fig. 1a,c).

To improve over simple LDA, in Fig. 2 we show the “experimental” bands with dispersions:

$$\begin{aligned} \epsilon(\mathbf{k}) = & t_0 + t_1 \left[2 \cos \frac{k_x}{2} \cos \frac{\sqrt{3} k_y}{2} + \cos k_x \right] + t_2 \left[2 \cos \frac{3k_x}{2} \cos \frac{\sqrt{3} k_y}{2} + \cos \sqrt{3} k_y \right] \\ & + t_3 \left[2 \cos k_x \cos \sqrt{3} k_y + \cos 2k_x \right] + t_4 \left[2 \cos 3k_x \cos \sqrt{3} k_y + \cos 2\sqrt{3} k_y \right], \end{aligned} \quad (1)$$

with hopping integrals t_i obtained from the fit to experimental Fermi surfaces [10]. Corresponding values of t_i (in eV) for Ta system are: for the band forming barrels around Γ and K points $t_0=-0.027$, $t_1=0.199$, $t_2=0.221$, $t_3=0.028$, $t_4=0.013$, for the band forming “bones” $t_0=0.407$, $t_1=0.114$, $t_2=0.444$, $t_3=-0.033$, $t_4=0.011$. For Nb system: for the band forming smaller cylinders $t_0=0.0003$, $t_1=0.0824$, $t_2=0.1667$, $t_3=0.0438$, $t_4=0.0158$, while for the band forming larger cylinders $t_0=0.1731$, $t_1=0.1014$, $t_2=0.2268$, $t_3=0.037$, $t_4=-0.0048$. These bands are used in further calculations below.

ELECTRONIC SCATTERING ON CDW

Commensurate CDW phase

Consider the schematic picture of the first Brillouin zone for two-dimensional hexagonal lattice, shown in Fig. 3. In hexagonal structures under study, the commensurate CDW vector is $\mathbf{Q} = \frac{2}{3}\Gamma M$ that corresponds to tripling the lattice period. Scattering an electron by this commensurate CDW vector returns electron back to equivalent point after triple scattering: $\epsilon(\mathbf{k} + 3\mathbf{Q}) = \epsilon(\mathbf{k})$. Moreover for hexagonal structures there are in fact six equivalent scattering vectors: $\mathbf{Q}_1 = (\frac{2}{3}, \frac{2}{3\sqrt{3}})\pi$, $\mathbf{Q}_2 = (\frac{2}{3}, \frac{2}{3\sqrt{3}})\pi$, $\mathbf{Q}_3 = (-\frac{2}{3}, \frac{2}{3\sqrt{3}})\pi$, and $\bar{\mathbf{Q}}_l = -\mathbf{Q}_l$ ($l = 1, 2, 3$). Maxima of Lindhardt function, calculated in Refs. [3, 10], are observed on these vectors \mathbf{Q} . In addition Lindhardt function shows pronounced maxima [3, 10] for vectors $\mathbf{X} = \frac{1}{2}\Gamma K$ ($\mathbf{X}_1 = (\frac{2}{3}, 0)\pi$, $\mathbf{X}_2 = (\frac{1}{3}, \frac{1}{\sqrt{3}})\pi$, $\mathbf{X}_3 = (-\frac{1}{3}, \frac{1}{\sqrt{3}})\pi$ and $\bar{\mathbf{X}}_l = -\mathbf{X}_l$ ($l = 1, 2, 3$)), which appear as sums of scattering vectors \mathbf{Q} (see Table I of momenta summation).

Thus an electron with momentum \mathbf{k} is scattered by any of thirteen different momenta (see Table I): $\mathbf{0}$ – preserving its initial momentum \mathbf{k} ; \mathbf{Q} (\mathbf{Q}_l and $\bar{\mathbf{Q}}_l$); \mathbf{X} (\mathbf{X}_l and $\bar{\mathbf{X}}_l$). Thus for one band case to find the diagonal Green's function of an electron $G(\mathbf{k}, \mathbf{k})$ and twelve off-diagonal ($G(\mathbf{k} \pm \mathbf{Q}_l, \mathbf{k})$ and ($G(\mathbf{k} \pm \mathbf{X}_l, \mathbf{k})$) single-electron Green's functions we have to solve the system of thirteen linear equations (17) (see Appendix). Such an approach can be generalized for a multiple band case with simplifying assumption [11] that intra- and interband CDW scattering amplitudes are just the same (see Appendix) Solving these equations we can finally find the diagonal Green function $G^{ij}(\mathbf{k}, \mathbf{k})$ ($i, j = 1, 2$ – band indices) and corresponding spectral function:

$$A(E, \mathbf{k}) = -\frac{1}{\pi} \text{Im} \sum_i G^{ii}(\mathbf{k}, \mathbf{k}) \quad (2)$$

determining the effective electron dispersion.

Incommensurate CDW phase

As was pointed above at temperature $T = 90$ K 2H-TaSe₂ (and 2H-NbSe₂ at 33.5K) undergoes phase transition into incommensurate CDW phase with scattering vector $\mathbf{Q} \sim 0.58 - 0.6\Gamma M$. Similar to the commensurate case discussed above, this vector corresponds to six independent scattering vectors $\mathbf{Q}_l, \bar{\mathbf{Q}}_l$ $l = 1, 2, 3$. Let us consider single scattering

TABLE I: Table of scattering vectors summation

	\mathbf{Q}_1	\mathbf{Q}_2	\mathbf{Q}_3	$\bar{\mathbf{Q}}_1$	$\bar{\mathbf{Q}}_2$	$\bar{\mathbf{Q}}_3$
\mathbf{Q}_1	$\bar{\mathbf{Q}}_1$	\mathbf{X}_2	\mathbf{Q}_2	0	$\bar{\mathbf{Q}}_3$	$\bar{\mathbf{X}}_1$
\mathbf{Q}_2	\mathbf{X}_2	$\bar{\mathbf{Q}}_2$	\mathbf{X}_3	\mathbf{Q}_3	0	\mathbf{Q}_1
\mathbf{Q}_3	\mathbf{Q}_2	\mathbf{X}_3	$\bar{\mathbf{Q}}_3$	$\bar{\mathbf{X}}_3$	$\bar{\mathbf{Q}}_1$	0
$\bar{\mathbf{Q}}_1$	0	\mathbf{Q}_3	$\bar{\mathbf{X}}_1$	\mathbf{Q}_1	$\bar{\mathbf{X}}_2$	$\bar{\mathbf{Q}}_2$
$\bar{\mathbf{Q}}_2$	$\bar{\mathbf{Q}}_3$	0	$\bar{\mathbf{Q}}_1$	$\bar{\mathbf{X}}_2$	\mathbf{Q}_2	$\bar{\mathbf{X}}_3$
$\bar{\mathbf{Q}}_3$	\mathbf{X}_1	\mathbf{Q}_1	0	$\bar{\mathbf{Q}}_2$	$\bar{\mathbf{X}}_3$	\mathbf{Q}_3

	\mathbf{Q}_1	\mathbf{Q}_2	\mathbf{Q}_3	$\bar{\mathbf{Q}}_1$	$\bar{\mathbf{Q}}_2$	$\bar{\mathbf{Q}}_3$
\mathbf{X}_1	$\bar{\mathbf{Q}}_2$	$\bar{\mathbf{Q}}_1$	\mathbf{Q}_1	$\bar{\mathbf{Q}}_3$	\mathbf{Q}_3	\mathbf{Q}_2
\mathbf{X}_2	\mathbf{Q}_3	$\bar{\mathbf{Q}}_3$	$\bar{\mathbf{Q}}_2$	\mathbf{Q}_2	\mathbf{Q}_1	$\bar{\mathbf{Q}}_1$
\mathbf{X}_3	$\bar{\mathbf{Q}}_2$	$\bar{\mathbf{Q}}_1$	\mathbf{Q}_1	$\bar{\mathbf{Q}}_3$	\mathbf{Q}_3	\mathbf{Q}_2
$\bar{\mathbf{X}}_1$	\mathbf{Q}_3	$\bar{\mathbf{Q}}_3$	$\bar{\mathbf{Q}}_2$	\mathbf{Q}_2	\mathbf{Q}_1	$\bar{\mathbf{Q}}_1$
$\bar{\mathbf{X}}_2$	$\bar{\mathbf{Q}}_2$	$\bar{\mathbf{Q}}_1$	\mathbf{Q}_1	$\bar{\mathbf{Q}}_3$	\mathbf{Q}_3	\mathbf{Q}_2
$\bar{\mathbf{X}}_3$	\mathbf{Q}_3	$\bar{\mathbf{Q}}_3$	$\bar{\mathbf{Q}}_2$	\mathbf{Q}_2	\mathbf{Q}_1	$\bar{\mathbf{Q}}_1$

of an electron with momenta \mathbf{k} near the FS by vector $\mathbf{Q}(\mathbf{Q}_l, \bar{\mathbf{Q}}_l)$. For general values of \mathbf{k} , such scattering act moves an electron quite far away from the FS, the only exception is an electron in the vicinity of the “hot-spots” where $\epsilon(\mathbf{k}+\mathbf{Q}) = \epsilon(\mathbf{k})$. Among multiple scattering processes most probable will be successive scattering processes by vectors \mathbf{Q}_l and $\bar{\mathbf{Q}}_l$ since in this case the scattered electron is back again to initial point with momenta \mathbf{k} close to the Fermi surface. To this end further we will work in the so called two-wave approximation, when scattering act consists of two successive scattering processes by vectors \mathbf{Q}_l and $\bar{\mathbf{Q}}_l$. Assuming that scattering amplitude is the same for intra- and interband transitions, for diagonal Green function’s we obtain (corresponding diagrammatic representation see in Fig. 4):

$$G^{ij}(\mathbf{k}, \mathbf{k}) = g^i(\mathbf{k})\delta_{ij} + g^i(\mathbf{k})\Sigma \sum_m G^{mj}(\mathbf{k}, \mathbf{k}), \quad (3)$$

where $\Sigma = \Delta^2 \sum_{jl} (g^j(\mathbf{k} + \mathbf{Q}_l) + g^j(\mathbf{k} - \mathbf{Q}_l))$ and $g^j(\mathbf{k}) = \frac{1}{E - \epsilon_j(\mathbf{k}) + i\delta}$ is bare retarded Green’s function for the n -th band. Summing Eq. (3) over i , one can get:

$$\sum_i G^{ij}(\mathbf{k}, \mathbf{k}) = \frac{g^j(\mathbf{k})}{1 - \Sigma \sum_i g^i(\mathbf{k})}. \quad (4)$$

Then using Eq. (3) again we obtain:

$$G^{ij}(\mathbf{k}, \mathbf{k}) = g^i(\mathbf{k})\delta_{ij} + \frac{g^i(\mathbf{k})\Sigma g^j(\mathbf{k})}{1 - \Sigma \sum_i g^i(\mathbf{k})}, \quad (5)$$

which can provide us with the spectral function (2) for the case of incommensurate CDW scattering.

CDW pseudogap fluctuations

Above the temperature of incommensurate CDW transition there is no long-range charge ordering, but due to low-dimensionality of the system there are rather well developed short-range order CDW fluctuations, with finite correlation length ξ and characteristic wave-vector \mathbf{Q} which becomes rather quick commensurate with $\mathbf{Q} = \frac{2}{3}\Gamma M$ [4] as temperature lowers. In analogy to incommensurate electronic CDW scattering we will employ two-wave approximation with pair of vectors $(\mathbf{Q}_l, \bar{\mathbf{Q}}_l)$. Diagrammatically such scattering processes are show in Fig. 5, where three types of interaction lines correspond to three characteristic transfer momenta $l = 1, 2, 3$.

Let us assume fluctuations Gaussian. Then averaging over such fluctuations corresponds to all possible interconnections of incoming and outgoing interaction lines of the same type [12–14], producing appropriate effective interactions, assumed to be of the form discussed in these works. For the case of high enough temperatures one can neglect dynamics of fluctuations and average over static random field of Gaussian pseudogap fluctuations [12–14].

Let us mention that the number of different diagrams is defined by product of number of ways to interconnect vertices of type 1, 2 and 3. Since only outgoing and incoming lines of each type can be connected, combinatorics corresponds to incommensurate case [12]. Following Refs. [12–14] we use the basic property of the diagrams of this model: any diagram with crossing interaction lines is equal to some noncrossing diagram of the same order. Thus only noncrossing diagrams can be considered, while contributions of *all* diagrams can be accounted by combinatorial prefactors. And for each type of interaction lines (1,2,3) we will have its own incommensurate combinatorial prefactors, same as in Refs. [12, 13].

Recurrent procedure for Green's function: single band case

Within some straightforward generalization of the approach of Refs. [12, 13], for single band case one-electron Green's function can be obtained via recurrent procedure, which is shown diagrammatically in Fig. 6. Here n_l is the number of interaction lines of type l

surrounding the “bare” electron line. Analytically this procedure can be written as:

$$G_{n_1, n_2, n_3}^{-1}(\mathbf{k}) = g_{n_1, n_2, n_3}^{-1}(\mathbf{k}) - \Sigma_{n_1+1, n_2, n_3} - \Sigma_{n_1, n_2+1, n_3} - \Sigma_{n_1, n_2, n_3+1}, \quad (6)$$

where n_1, n_2, n_3 – are even and

$$\Sigma_{n_1+1, n_2, n_3} = \Delta^2 s(n_1 + 1)[G_{n_1+1, n_2, n_3}(\mathbf{k} + \mathbf{Q}_1) + G_{n_1+1, n_2, n_3}(\mathbf{k} - \mathbf{Q}_1)]. \quad (7)$$

The other self-energies Σ in (6) can be found similarly to (7), but n_2 or n_3 should be increased by one and vectors \mathbf{Q}_2 or \mathbf{Q}_3 should be added (subtracted) to (from) \mathbf{k} , while

$$G_{n_1+1, n_2, n_3}^{-1}(\mathbf{k} \pm \mathbf{Q}_1) = g_{n_1+1, n_2, n_3}^{-1}(\mathbf{k} \pm \mathbf{Q}_1) - \Sigma_{n_1+2, n_2, n_3}, \quad (8)$$

and

$$\Sigma_{n_1+2, n_2, n_3} = \Delta^2 s(n_1 + 2)G_{n_1+2, n_2, n_3}(\mathbf{k}). \quad (9)$$

Here

$$g_{n_1, n_2, n_3}(\mathbf{k}) = \frac{1}{E - \epsilon(\mathbf{k}) + inv(\mathbf{k})\kappa}, \quad (10)$$

and $\kappa = 1/\xi$ is the inverse correlation length of pseudogap fluctuations, $n = n_1 + n_2 + n_3$, $v(\mathbf{k}) = |v_x(\mathbf{k}) + v_y(\mathbf{k})|$, $v_{x,y}(\mathbf{k}) = \frac{\partial \epsilon(\mathbf{k})}{\partial k_{x,y}}$ are projections of quasiparticle velocities.

For the case of incommensurate fluctuations, combinatorial prefactors are:

$$s(n) = \begin{cases} \frac{n+1}{2} & \text{for odd } k \\ \frac{n}{2} & \text{for even } k \end{cases} \quad (11)$$

This recurrent procedure is applied in analogy with refs. [12, 13]. As a first step, one takes large enough $n = n_1 + n_2 + n_3$, for example even, and assume that *all* Green functions G_{n_1, n_2, n_3} with even n_1, n_2, n_3 , such that $n = n_1 + n_2 + n_3$ are equal to zero. Then from (9) one can find that all Σ_{n_1, n_2, n_3} for the same indices are equal to zero too. Then using recurrent procedure, one can get *all* new values for G_{n_1, n_2, n_3} with even n_1, n_2, n_3 , such that $n_1 + n_2 + n_3 = n - 2$, and repeat the recurrent procedure until one obtains physical Green function:

$$G(\mathbf{k}) = G_{0,0,0}(\mathbf{k}). \quad (12)$$

Multiple bands pseudogap model for quasi two dimensional hexagonal structures.

In hexagonal diselenides TaSe₂ and NbSe₂, as we have seen, the Fermi level is crossed by two bands. Thus, our recurrent procedure should be generalized for multiple bands. We

will follow Ref. [11], devoted to description of possible pseudogap behavior in iron based superconductors, and assume that intra and interband pseudogap scattering amplitudes are identical. This simplifies further analysis and the recurrent procedure for diagonal elements of the general matrix (over band indices) Green's function G^{ij} can be drawn diagrammatically as in Fig. 7. For our two band model each of the band indices run over two possible values, and there is summation over all possible values of indices p, m, l in the vertices (Fig. 7). Thus, the self-energy in these diagrams has no dependence on band indices at all and we can obtain the recurrent procedure for $G_{n_1, n_2, n_3} = \sum_{i, j} G_{n_1, n_2, n_3}^{ij}$, which is identical to Eqs. (6)-(9) as in single band case, with only replacement:

$$g_{n_1, n_2, n_3}(\mathbf{k}) = \sum_i g_{n_1, n_2, n_3}^i(\mathbf{k}) = \sum_j \frac{1}{E - \epsilon_j(\mathbf{k}) + inv_j(\mathbf{k})\kappa} \quad n = n_1 + n_2 + n_3. \quad (13)$$

and at the end of the procedure we define the physical matrix Green function as:

$$G^{ij}(\mathbf{k}) = g_{0,0,0}^i(\mathbf{k})\delta_{ij} + \frac{g_{0,0,0}^i(\mathbf{k})\Sigma g_{0,0,0}^j(\mathbf{k})}{1 - \Sigma g_{0,0,0}(\mathbf{k})}, \quad (14)$$

where $\Sigma = \Sigma_{1,0,0} + \Sigma_{0,1,0} + \Sigma_{0,0,1}$. This Green's function allows us to find the spectral function (2) in the presence of CDW pseudogap fluctuations.

RESULTS AND DISCUSSION

In our calculations we used rather typical estimate of CDW potential $\Delta = 0.05$ eV, and for correlations length of pseudogap fluctuations we assumed the value of $\xi = 10a$ (where a is the lattice spacing). To mimic for the experimental ARPES resolution we broadened our spectral functions with Lorentzian of width $\gamma = 0.03eV$, practically it means that we made substitution $E \rightarrow E + i\gamma$ during all calculations.

In Fig. 8 we show spectral function maps along high symmetry directions with $k_z = 0$ for 2H-TaSe₂. Upper panel shows spectral function map for incommensurate pseudogap phase obtained within our pseudogap model. In general it reminds bare "experimental" dispersions plotted on Fig. 2. However, here we see some *additional* broadening of initial spectra. These broadened regions of spectral functions with lower intensity represent regions pseudogap formation. Why do we speak about regions? In contrast to cuprates [15] where we have finite and rather small number of "hot-spots" here we have almost infinite number

of “hot-spots” and it is the interplay between all of them, which leads to the formation of such regions. But still dispersions here does not have any obvious discontinuities.

Middle panel of Fig. 8 displays the case of incommensurate CDW phase. Now we see that regions previously covered with pseudogap have clear discontinuities – gaps and also many shadow bands. When we transfer further to commensurate CDW phase (lower panel of Fig.8) those gaps become even stronger and we can see much more pronounced shadow bands.

Figures 9–11 show spectral functions maps in the vicinity of the Fermi level along cuts shown on Fig. 1c. In all figures upper row represents experimental data of Ref. [4], while lower shows our theoretical results. Generally speaking for all phases: incommensurate pseudogap Fig. 9, incommensurate CDW Fig. 10 and commensurate CDW Fig. 11, we obtain quite good qualitative agreement of theory and experiment for the number of bands crossing the Fermi level, their position and relative intensity.

In Fig. 12 we present comparison of experimental and theoretical Fermi surfaces for 2H-TaSe₂. In the middle part of Fig. 12 we show experimental ARPES data from Ref. [4]. Data at 180K corresponds to the pseudogap phase, while those at 30K are for commensurate CDW phase.

Upper panel of Fig. 12 shows our theoretical Fermi surface in the incommensurate pseudogap regime for 2H-TaSe₂. In general it more or less reminds LDA Fermi surface from Fig. 1c. However there are obvious signatures of partial destruction of the Fermi surface sheets. Namely, cylinder around K-point and “bones” along K-M direction are partially smeared out. It is seen that this picture agrees well with the experimental ARPES data of Ref. [3, 4].

For the commensurate CDW phase (lower panel of Fig. 12) Fermi surface stays close to that obtained in LDA and shown in of Fig. 1c. In contrast to incommensurate pseudogap phase Fermi surface sheets here are more sharp both in experiment and in theory. The cylinder around K-point is now continuous. In the middle of the “bones” we observe the start of formation of small triangles as shown in the center of middle panel. Thus, here in commensurate CDW phase of 2H-TaSe₂ we again obtain an overall agreement between theory and experiment.

In Fig. 13 we show comparison between experimental (middle panel) and theoretical Fermi surfaces (lower and upper panel) for 2H-NbSe₂. Experimental data on the Fermi surface are available only for commensurate CDW phase [5]. Thus we can compare these

with theoretical picture shown on lower panel of Fig. 13. In general, both Fermi surfaces remind those from Fig. 1b. Account of electron scattering on commensurate CDW leads to a small regions of Fermi surface destruction, namely, along Γ -K and K-M directions. If there exists incommensurate pseudogap phase for 2H-NbSe₂ at high enough temperatures, its Fermi surface will not be changed much by pseudogap fluctuations, as seen in the upper panel of Fig. 13).

CONCLUSION

To conclude, here we presented theoretical results on electronic structure of two-dimensional diselenides 2H-TaSe₂ and 2H-NbSe₂ within different CDW phases.

First of all we formulated a theoretical approach to account for multiple scattering of electrons on different types of CDW, also for the multiple bands case. Further we investigated spectral functions and Fermi surfaces for the pseudogap, incommensurate CDW and commensurate CDW phases. Calculated theoretical spectral functions within the pseudogap phase demonstrate “hot regions”, where spectral function is additionally broadened. In incommensurate CDW and commensurate CDW phases in a place of these “hot regions” we obtained opening of the number of gaps at the intersections with rather pronounced “shadow bands”. Comparing experimental and theoretical Fermi surfaces in the pseudogap phase we observe rather clear signs of partial Fermi surface destruction with formation of a number of typical “Fermi arcs”, separated by pseudogap regions. In commensurate CDW phase Fermi surfaces are rather similar to initial LDA picture, with pretty small features due to CDW. The overall agreement between theory and ARPES experiments is rather satisfactory.

ACKNOWLEDGEMENTS

We thank S.V. Borisenko for his interest and helpful discussions. This work is partly supported by RFBR grant 11-02-00147 and was performed within the framework of Programs of Fundamental Research of the Russian Academy of Sciences (RAS) “Quantum physics of condensed matter” (UB RAS 09-II-2-1009) and of the Physics Division of RAS “Strongly correlated electrons in solid states” (UB RAS 09-T-2-1011).

Appendix: Scattering on commensurate CDW

One band scattering

First let us consider single band case with electronic “bare” spectrum $\epsilon(\mathbf{k})$. These “bare” electrons are scattered on CDW potential, written as:

$$V(\mathbf{r}) = 2\Delta \sum_{l=1}^3 \cos \mathbf{Q}_l \mathbf{r}. \quad (15)$$

“Bare” retarded Green’s function is:

$$g(\mathbf{k}) = \frac{1}{E - \epsilon(\mathbf{k}) + i\delta}. \quad (16)$$

Let us introduce short notations: $g(\mathbf{k}) = g$; $g(\mathbf{k} + \mathbf{Q}_l) = f_l$; $g(\mathbf{k} - \mathbf{Q}_l) = f_{\bar{l}}$; $g(\mathbf{k} + \mathbf{X}_l) = \phi_l$; $g(\mathbf{k} - \mathbf{X}_l) = \phi_{\bar{l}}$. Then for diagonal Green’s function $G = G(\mathbf{k}, \mathbf{k})$ and twelve off-diagonal ($F_l = G(\mathbf{k} + \mathbf{Q}_l, \mathbf{k})$; $F_{\bar{l}} = G(\mathbf{k} - \mathbf{Q}_l, \mathbf{k})$; $\Phi_l = G(\mathbf{k} + \mathbf{X}_l, \mathbf{k})$; $\Phi_{\bar{l}} = G(\mathbf{k} - \mathbf{X}_l, \mathbf{k})$) one can get the following system of thirteen linear equations (see Table I of scattering vectors summation):

$$\begin{aligned} G &= g + g\Delta F \\ F_1 &= f_1\Delta(F_{\bar{1}} + \Phi_2 + F_2 + G + F_3 + \Phi_1) \\ F_2 &= f_2\Delta(\Phi_2 + F_2 + \Phi_3 + F_3 + G + F_1) \\ F_3 &= f_3\Delta(F_2 + \Phi_3 + F_3 + \Phi_{\bar{1}} + F_{\bar{1}} + G) \\ F_{\bar{1}} &= f_{\bar{1}}\Delta(G + F_3 + \Phi_{\bar{1}} + F_1 + \Phi_{\bar{2}} + F_{\bar{2}}) \\ F_{\bar{2}} &= f_{\bar{2}}\Delta(F_3 + G + F_{\bar{1}} + \Phi_{\bar{2}} + F_2 + \Phi_{\bar{3}}) \\ F_{\bar{3}} &= f_{\bar{3}}\Delta(\Phi_{\bar{1}} + F_1 + G + F_{\bar{2}} + \Phi_{\bar{3}} + F_3) \\ \Phi_l &= \phi_l\Delta F; \quad \Phi_{\bar{l}} = \phi_{\bar{l}}\Delta F, \end{aligned} \quad (17)$$

where $F = \sum_{l=1}^3 (F_l + F_{\bar{l}})$.

Solving Eqs. (17), one can the get diagonal Green’s function $G = G(\mathbf{k}, \mathbf{k})$:

$$G = gK; \quad K = \frac{1 - \alpha\beta - a(\beta + 1) - b(\alpha + 1)}{1 - \alpha\beta - a(\beta + 1) - b(\alpha + 1) - g\Delta[\alpha(\beta + 1) + \beta(\alpha + 1)]}, \quad (18)$$

where $\alpha = \Delta(f_2 + f_{\bar{1}} + f_{\bar{3}})$, $\beta = \Delta(f_1 + f_3 + f_{\bar{2}})$, $a = \Delta^2[f_{\bar{1}}(\phi_{\bar{1}} + \phi_{\bar{2}}) + f_2(\phi_2 + \phi_3) + f_{\bar{3}}(\phi_{\bar{3}} + \phi_1)]$, $b = \Delta^2[f_1(\phi_1 + \phi_2) + f_3(\phi_3 + \phi_{\bar{1}}) + f_{\bar{2}}(\phi_{\bar{2}} + \phi_{\bar{3}})]$.

Multiband scattering

Following the approach of Ref. [11] we assume that CDW scattering amplitude Δ is identical for intra and interband transitions. One can define short notations: $g^i = g^i(\mathbf{k}) = \frac{1}{E - \epsilon_i(\mathbf{k}) + i\delta}$; $f_{l(\bar{l})}^i = g^i(\mathbf{k} \pm \mathbf{Q}_l)$; $\phi_{l(\bar{l})}^i = g^i(\mathbf{k} \pm \mathbf{X}_l)$, where i – band index. Diagonal and off-diagonal Green's functions will have additional band indices. The rest of notations are the same as for single band case. For diagonal Green's function, in analogy with first equation of the system (17), one can obtain:

$$G^{ij} = g^i \delta_{ij} + g^i \Delta \sum_m \sum_{l=1}^3 (F_l^{mj} + F_{\bar{l}}^{mj}). \quad (19)$$

Introducing $G^j = \sum_i G^{ij}$; $F_{l(\bar{l})}^j = \sum_i F_{l(\bar{l})}^{ij}$; $\Phi_{l(\bar{l})}^j = \sum_i \Phi_{l(\bar{l})}^{ij}$; $g = \sum_i g^i$; $f_{l(\bar{l})} = \sum_i f_{l(\bar{l})}^i$; $\phi_{l(\bar{l})} = \sum_i \phi_{l(\bar{l})}^i$ and summing Eq. (19) over i we get:

$$G^j = g^j + g \Delta \sum_{l=1}^3 (F_l^j + F_{\bar{l}}^j). \quad (20)$$

The rest of other twelve equations for $F_{l(\bar{l})}^j$ and $\Phi_{l(\bar{l})}^j$ are completely equivalent to corresponding equations of one band case (17). Thus, we immediately obtain:

$$G^j = g^j K, \quad (21)$$

where K is defined in Eq. (18). However, now the quantities g , $f_{l(\bar{l})}$, $\phi_{l(\bar{l})}$ are summed up over all band indices. From Eq. (19) and (20), using Eq. (21) we finally obtain:

$$G^{ij} = g^i \delta_{ij} + g^i \frac{G^j - g^j}{g} = g^i \delta_{ij} + \frac{g^i g^j}{g} (K - 1), \quad (22)$$

which allows us to calculate the spectral function (2) with the account of scattering on commensurate CDW.

-
- [1] J.A. Wilson, F.J. Di Salvo, S. Mahajan, *Adv. Phys.* **24**, 117 (1975).
- [2] D.E. Moncton, J.D. Axe, and F.J. Di Salvo, *Phys. Rev. Lett.* **34**, 734 (1975); *Phys. Rev. B* **16**, 801 (1977).
- [3] D. S. Inosov, V. B. Zabolotnyy, D. V. Evtushinsky, A. A. Kordyuk, B. Buchner, R. Follath, H. Berger, and S. V. Borisenko *New J. Phys.* **10**, 125027 (2008).
- [4] S. V. Borisenko, A. A. Kordyuk, A. N. Yaresko, V. B. Zabolotnyy, D. S. Inosov, R. Schuster, B. Buchner, R. Weber, R. Follath, L. Patthey, H. Berger. *Phys. Rev. Lett.* **100**, 196402 (2008).
- [5] S. V. Borisenko, A. A. Kordyuk, V. B. Zabolotnyy, D. S. Inosov, D. Evtushinsky, B. Buchner, A. N. Yaresko, A. Varykhalov, R. Follath, W. Eberhardt, L. Patthey, H. Berger. *Phys. Rev. Lett.* **102**, 166402 (2009)
- [6] O.K. Andersen. *Phys. Rev. B* **12**, 3060 (1975); O. Gunnarsson, O. Jepsen, O.K. Andersen. *Phys. Rev. B* **27**, 7144 (1983); O.K. Andersen, O. Jepsen. *Phys. Rev. Lett.* **53**, 2571 (1984).
- [7] R.A. Bromley, *Phys. Rev. Lett.* **29**, 357 (1972); L.F. Mattheiss, *Phys. Rev. B* **8**, 3719 (1973); G. Wexler, A.M. Wooley *J. Phys. C: Solid State Phys.* **9**, 1185 (1976); R. Corcoran *et al.*, *J. Phys.: Condens. Matter* **6**, 4479 (1994); H.E. Brauer *et al.*, *J. Phys.: Condens. Matter* **13**, 9879 (2001); M.-T. Suzuki, H. Harima, *Physica B*, **359-361**, 1180 (2004).
- [8] N.V. Smith, S.D. Kevan, F.J. Di Salvo, *J. Phys. C: Solid State Phys.* **18**, 3175 (1985).
- [9] K. Rossnagel, E. Rotenberg, H. Koh, N.V. Smith, and L. Kipp, *Phys. Rev. B* **72**, 121103 (2005).
- [10] D. S. Inosov, D. V. Evtushinsky, V. B. Zabolotnyy, A. A. Kordyuk, B. Buchner, R. Follath, H. Berger, S. V. Borisenko. *Phys. Rev. B* **79**, 125112 (2009).
- [11] E.Z.Kuchinskii, M.V.Sadovskii. *Pis'ma v ZhETF* **91**, 729 (2010) [*JETP Lett.* **91**, 660 (2010)].
- [12] M.V.Sadovskii. *Zh. Eksp. Teor. Fiz.* **66**, 1720 (1974) [*Sov. Phys. - JETP* **39**, 845 (1974)]; *Zh. Eksp. Teor. Fiz.* **77**, 2070 (1979) [*Sov. Phys. - JETP* **50**, 989 (1979)].
- [13] E.Z. Kuchinskii, M.V. Sadovskii, *Zh. Eksp. Teor. Fiz.* **115**, 1765 (1999) [*JETP* **88**, 968 (1999)].
- [14] J. Schmalian, D. Pines, B. Stojkovic. *Phys. Rev. Lett.* **80**, 3839(1998); *Phys. Rev. B* **60**, 667 (1999).

- [15] M.V. Sadvskii, Usp. Fiz. Nauk **171**, 539 (2001) [Physics-Uspekhi **44**, 515 (2001)];
Also in *Strings, branes, lattices, networks, pseudogaps and dust* (Moscow:Scientific World,
2007) p. 357 (in Russian, English version – ArXiv: cond-mat/0408489).

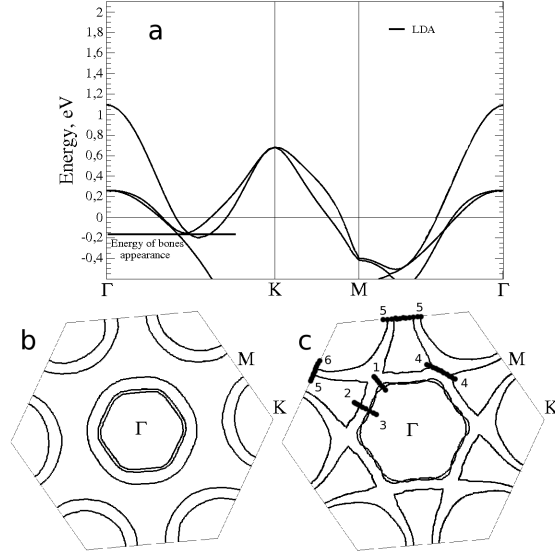


FIG. 1: LDA bands and Fermi surfaces for 2H-TaSe₂. Panel (a) – LDA electronic dispersions. Fermi level corresponds to zero. Panel (b) – LDA Fermi surface. Panel (c) – Fermi surface for shifted down Fermi level shown on panel (a) with a short line to obtain bone-like Fermi sheets.

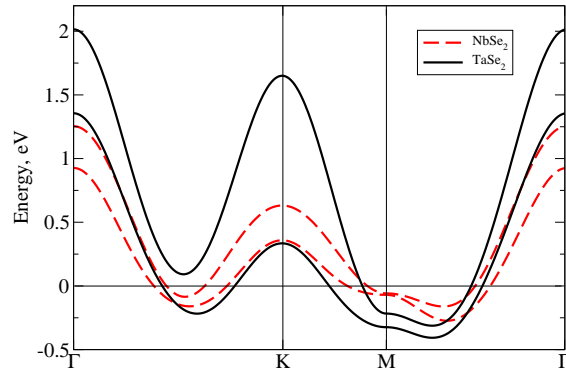


FIG. 2: “Experimental” bands for 2H-TaSe₂ (solid line) and 2H-NbSe₂ (dashed line). Fermi level corresponds to zero.

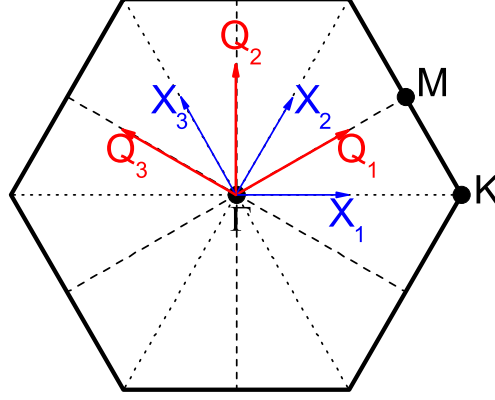


FIG. 3: Schematic picture of the first Brillouin zone for hexagonal lattice with characteristic CDW vectors: $\mathbf{Q} = \frac{2}{3}\Gamma M$ ($\mathbf{Q}_1, \mathbf{Q}_2, \mathbf{Q}_3$) – commensurate CDW vectors. $\mathbf{X} = \frac{1}{2}\Gamma K$ ($\mathbf{X}_1, \mathbf{X}_2, \mathbf{X}_3$) – vectors after two scattering on \mathbf{Q} , which also have significant Lindhardt function maxima.[3]

$$\frac{i}{\mathbf{k}} \frac{j}{\mathbf{k}} = \frac{i}{\mathbf{k}} \frac{i}{\mathbf{k}} + \frac{i}{\mathbf{k}} \overset{\Delta}{\underset{\zeta n}{\sim}} \frac{n}{\mathbf{k} \pm \mathbf{Q}_1} \overset{\Delta}{\underset{\zeta m}{\sim}} \frac{j}{\mathbf{k}} \frac{j}{\mathbf{k}}$$

FIG. 4: Diagrammatic representation of diagonal Green function within two-wave approximation for electron scattering on CDW.

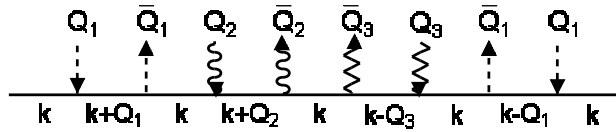


FIG. 5: Example of a diagram with multiple scattering on CDW, where dashed, wavy and zig-zag lines incoming lines corresponds to scattering on $\mathbf{Q}_1, \mathbf{Q}_2, \mathbf{Q}_3$, and corresponding outgoing lines – $\bar{\mathbf{Q}}_1, \bar{\mathbf{Q}}_2, \bar{\mathbf{Q}}_3$.

$$\begin{aligned}
\frac{k}{n_1 n_2 n_3} &= \frac{k}{n_1 n_2 n_3} + \frac{k}{n_1 n_2 n_3} \overset{\Delta^2 s(n_1+1)}{\text{---} \overset{k+Q_1}{\text{---}} \text{---}} \frac{k}{n_1 n_2 n_3} + \frac{k}{n_1 n_2 n_3} \overset{\Delta^2 s(n_1+1)}{\text{---} \overset{k-Q_1}{\text{---}} \text{---}} \frac{k}{n_1 n_2 n_3} + (1 \rightarrow 2) + (1 \rightarrow 3) \\
\frac{k \pm Q_1}{n_1+1 n_2 n_3} &= \frac{k \pm Q_1}{n_1+1 n_2 n_3} + \frac{k \pm Q_1}{n_1+1 n_2 n_3} \overset{\Delta^2 s(n_1+2)}{\text{---} \overset{k}{\text{---}} \text{---}} \frac{k \pm Q_1}{n_1+1 n_2 n_3}
\end{aligned}$$

$n_1, n_2, n_3 - \text{even}$

FIG. 6: Diagrammatic representation of Green function within single band pseudogap model for two dimensional hexagonal systems. (1 \rightarrow 2) denotes the two last terms, where substitutions $Q_1 \rightarrow Q_2$ and $n_1 + 1 \rightarrow n_2 + 1$ should be done.

$$\begin{aligned}
\frac{i \ k \ j}{n_1 n_2 n_3} &= \frac{i \ k \ j}{n_1 n_2 n_3} + \frac{\Delta^2 s(n_1+1)}{n_1 n_2 n_3} \frac{i \ k \ j}{n_1+1 n_2 n_3} \frac{\Delta^2 s(n_1+1)}{n_1 n_2 n_3} \frac{i \ k \ j}{n_1 n_2 n_3} + \frac{\Delta^2 s(n_1+1)}{n_1 n_2 n_3} \frac{i \ k \ j}{n_1+1 n_2 n_3} \frac{\Delta^2 s(n_1+1)}{n_1 n_2 n_3} \frac{i \ k \ j}{n_1 n_2 n_3} + (1 \rightarrow 2) + (1 \rightarrow 3) \\
\frac{i \ k \pm Q_1 j}{n_1+1 n_2 n_3} &= \frac{i \ k \pm Q_1 j}{n_1+1 n_2 n_3} + \frac{\Delta^2 s(n_1+2)}{n_1+1 n_2 n_3} \frac{i \ k \pm Q_1 j}{n_1+2 n_2 n_3} \frac{\Delta^2 s(n_1+2)}{n_1+1 n_2 n_3} \frac{i \ k \pm Q_1 j}{n_1+1 n_2 n_3}
\end{aligned}$$

n_1, n_2, n_3 - even

FIG. 7: Diagrammatic representation of Green function within multiband pseudogap model for two dimensional hexagonal systems.

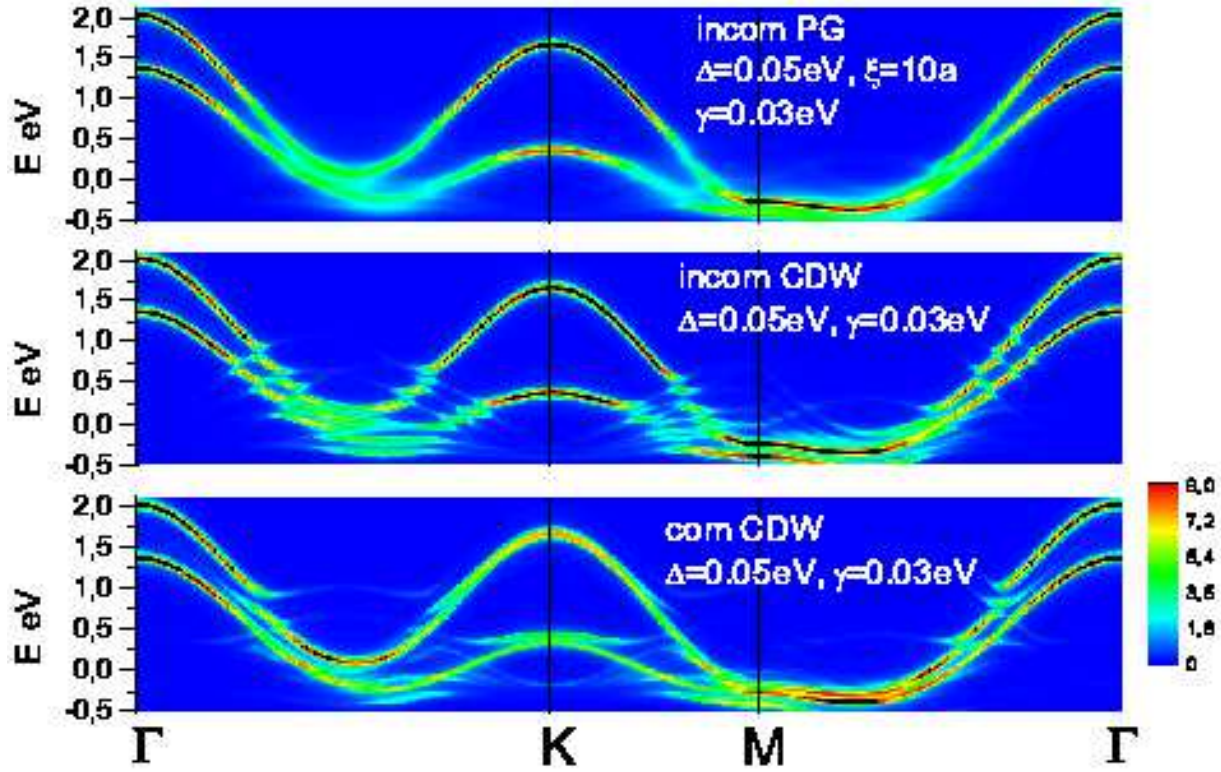


FIG. 8: Spectral functions of 2H-TaSe₂. Upper panel – incommensurate pseudogap phase, middle panel – incommensurate CDW phase, lower panel – commensurate CDW phase.

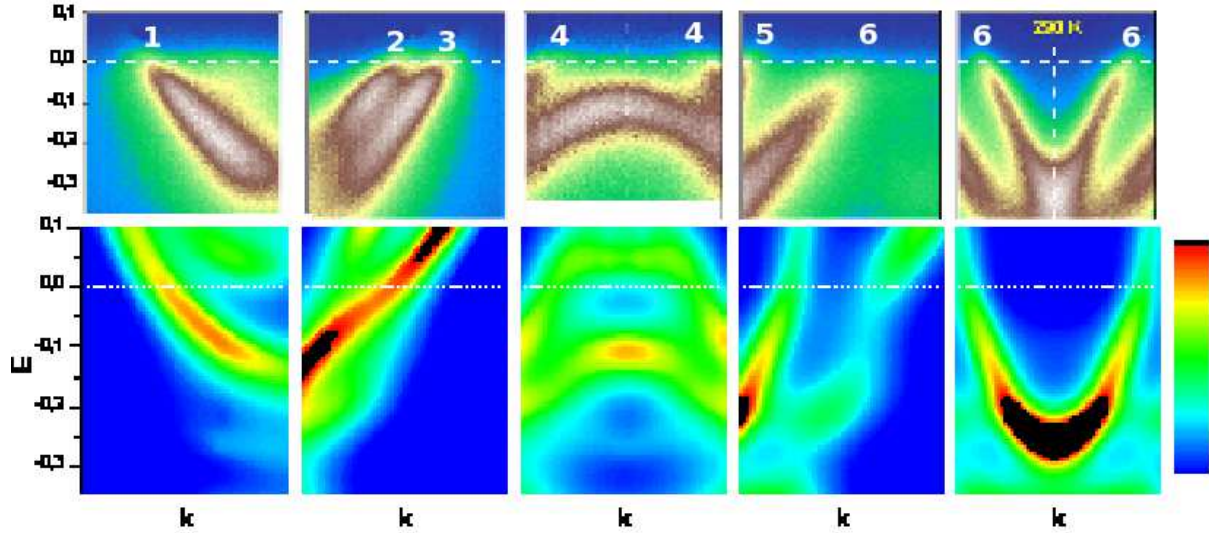


FIG. 9: Spectral functions for incommensurate pseudogap phase along cuts shown on Fig. 1c

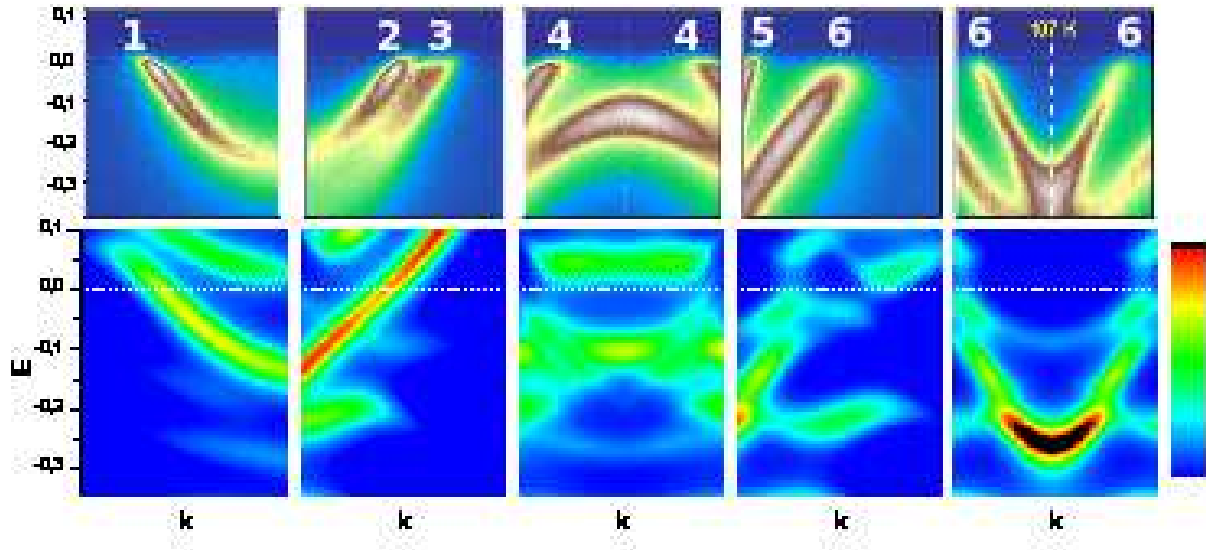


FIG. 10: The same as Fig. 9 but for incommensurate CDW phase.

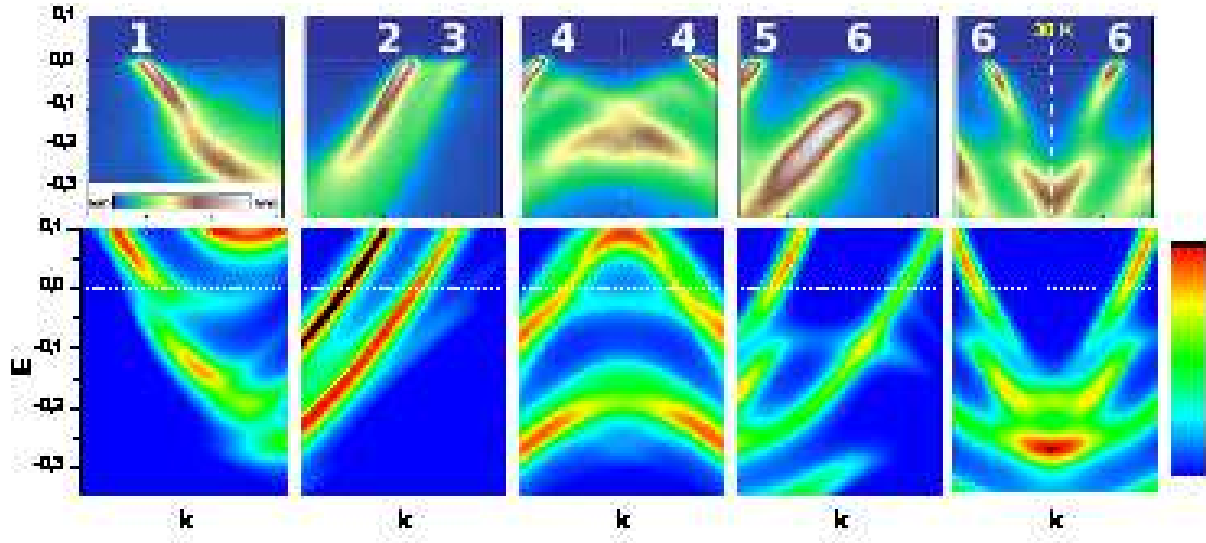


FIG. 11: The same as Fig. 9 but for commensurate CDW phase.

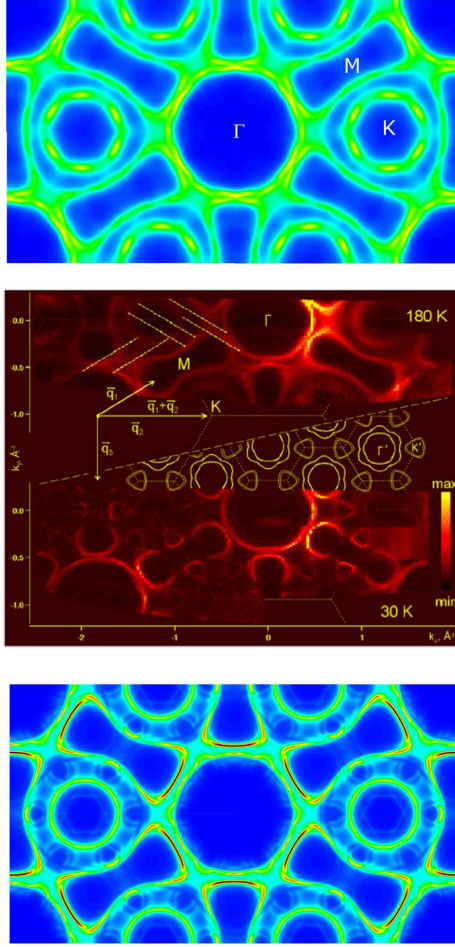


FIG. 12: Comparison of experimental and theoretical Fermi surfaces for 2H-TaSe₂. Upper panel – theoretical Fermi surface for pseudogap CDW phase; middle panel – joint picture of experimental data pseudogap phase (upper part) and commensurate CDW phase (lower part). Lower panel – theoretical Fermi surface for commensurate CDW phase.

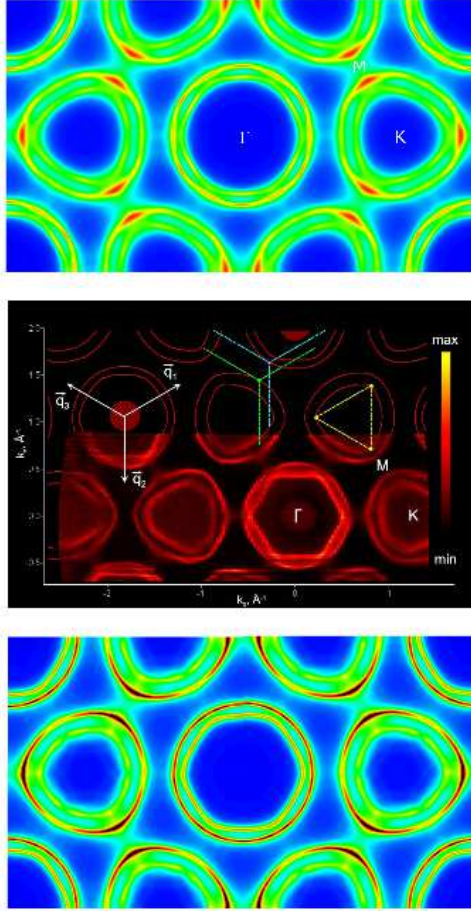


FIG. 13: Comparison of experimental and theoretical Fermi surfaces for 2H-NbSe₂. Upper panel – theoretical Fermi surface for pseudogap CDW phase; middle panel – joint picture of experimental data LDA Fermi surface (upper part) and commensurate CDW phase (lower part). Lower panel – theoretical Fermi surface for commensurate CDW phase.